Article:
Califano, M and Rodosthenous, P (2018) Theoretical Characterization of GaSb Colloidal Quantum Dots and Their Application to Photocatalytic CO_2 Reduction with Water. ACS Applied Materials & Interfaces, 11 (1). pp. 640-646. ISSN: 1944-8244

https://doi.org/10.1021/acsami.8b15492

Theoretical Characterisation of GaSb Colloidal Quantum Dots and their Application to Photocatalytic CO_2 Reduction with Water

Marco Califano* and Panagiotis Rodosthenous

Pollard Institute, School of Electronic and Electrical Engineering, University of Leeds, Leeds LS2 9JT, United Kingdom

E-mail: m.califano@leeds.ac.uk

Abstract

With a large exciton Bohr radius and a high hole mobility in the bulk, GaSb is an important semiconductor material for technological applications. Here we present a theoretical investigation into the evolution of some of its most fundamental characteristics at the nanoscale. GaSb emerges as a widely tunable, potentially disruptive new colloidal material with huge potential for application in a wide range of fields.

Keywords: *Nanocrystals, colloidal quantum dots, GaSb, pseudopotential method, k-vector analysis, direct-to-indirect transitions*

Introduction

In the past three decades there has been growing interest in GaSb as both substrate and active device material, owing to its peculiar structural, electronic and thermal properties.[1]

*To whom correspondence should be addressed

GaSb-based structures have been proposed for a wide range of applications from high-speed optoelectronics[2–8] to high-efficiency solar energy conversion[9,10] from gas sensing and environmental monitoring,[1] to biomedical imaging and health care.[11]

Epitaxial structures of reduced dimensionality, such as GaSb/AlGaSb quantum wells, are characterised by optical transitions in the wavelength region of technological importance for optical communication systems. They have found application in infrared optics as lasers, photodetectors[12,13] and gas sensors,[14] whereas GaSb nanowires, owing to the high hole mobility in GaSb, are being exploited in III-V p-channel metal-oxide-semiconductor field-effect transistors (MOSFETs).[15,16] GaSb/GaAs quantum dots (QDs), thanks to the quasi-type II band alignment at the heterointerface which confines the hole to the QD and leaves the electron in the matrix loosely bound by the Coulomb interaction with the hole, are ideally suited for a variety of fast, low power electronic devices and infrared light sources,[17,18] as well as for light-emitting devices in the spectral range 1-1.5 μm, with applications in biomedical imaging in ophthalmology, neurology, and endoscopy.[19] GaSb 0D systems are also attractive materials for quantum dot infrared photodetectors (QDIPs) and quantum dot field effect transistors (QD-FET), with possible applications in quantum communications and night vision. Another interesting application for GaSb/GaAs QDs is in charge-based memories.[20–23] In a QD-memory (QDM), charge is captured (and stored) in a potential well, which may be created by either the valence or the conduction band offset between dot and matrix material. The peculiar band alignment in GaSb/GaAs QDs is such that the difference in band gap between the two materials is taken up entirely by the valence band, yielding confinement energies for the hole of the order of 600 meV.[22] The latter are directly linked to the maximum charge-storage time t_s achievable in the system, which has been shown to increase by one order of magnitude for each 50 meV of additional well depth (confinement energy).[22] Considering that a hole confinement of 600 meV was estimated to yield a room-temperature charge-storage time of the order of 0.2 ms,[22] and that the target charge-storage time for a non-volatile memory is in excess of a decade, confinements in excess of 1.1 eV

will be needed to achieve it. Whilst such a depth for the hole potential well is difficult (if not impossible) to achieve in an *epitaxial* dot, this is the order of magnitude of charge confinement commonly exhibited by *colloidal* quantum dots (CQDs).[24]

Here we present a theoretical characterisation study on precisely these nanostructures, which, based on the properties exhibited by their epitaxial counterparts, are expected to be promising candidates for a variety of device applications. We consider GaSb nanocrystals (NCs) with radii ranging from 11 to 45 Å, containing from 175 to over 13000 atoms. Given the large bulk Bohr radius of GaSb (20.46 nm) and its peculiar band structure, exhibiting closely spaced minima in the conduction band (CB) where the minimum at Γ and the slightly higher minima at the L-points are only about 80 meV apart, whereas the ratio of their respective effective masses is larger than 2,[25] it is expected that confinement should induce a Γ-to-L transition in the character of the conduction band minimum, similarly to what was predicted to occur in GaAs,[26] where the Γ-L and Γ-X separations are much larger (300 eV and 460 eV, respectively), and the bulk Bohr radius is nearly one half (11.6 nm) than in GaSb. The valence band of GaSb, instead, has the structure common to all zincblende semiconductors, hence its Γ character is not expected to change with confinement. As a consequence, a confinement-induced direct-to-indirect band gap transition is expected in this material, which should lead to long exciton storage times in GaSb NQDs of suitably small sizes. This, coupled with the high hole mobility in the bulk, could make GaSb nanocrystals ideal building blocks for a wide range of optoelectronic applications.

Method

The CQD modelled in this work are assumed to have a bulk-like crystal structure and are built starting from a central anion, up to the desired radius. This procedure yields unsaturated bonds at the dot surface, which are passivated here by pseudo-hydrogenic, short-range potentials with Gaussian form.[27] The single-particle energies and wave functions are obtained

using the Pescan code,[28] based on the plane-wave semiempirical pseudopotential method described in Ref. [29], including spin-orbit coupling (we use the GaSb pseudopotentials derived by Magri and Zunger[30]). The excitonic spectra are obtained via a configuration interaction (CI) scheme,[31,32] using up to 14 conduction and 17 valence states, corresponding to a CI basis set of 952 configurations, covering a window of about 200 meV above the ground state exciton. The thermally averaged radiative lifetimes are calculated in the framework of standard time-dependent perturbation theory[33,34] assuming a Boltzmann occupation of higher-energy excitonic levels

$$\frac{1}{\tau(T)} = \frac{\sum_i (1/\tau_i) e^{-(E_i - E_0)/k_B T}}{\sum_i e^{-(E_i - E_0)/k_B T}} \tag{1}$$

where T is the temperature, k_B the Boltzmann constant, E_i the energy of the exciton in state i ($i = 0, \ldots, n$), τ_i is the intrinsic lifetime, defined as[35]

$$\frac{1}{\tau_i} = \frac{4nF^2\alpha\omega_i^3}{3c^2} |M_i|^2, \tag{2}$$

n is the refractive index of the medium surrounding the nanocrystal (here we use n=1.497 for toluene), $F = 3\epsilon/(\epsilon_{NC} + 2\epsilon)$ is the screening factor, $\epsilon = n^2$, ϵ_{NC} is the size-dependent dielectric constant of the NC calculated using a modified Penn model,[31] α is the fine-structure constant, $\hbar\omega_i$ is the transition energy, c is the speed of light in vacuum, and M_i is the CI dipole matrix element.[34]

The k-space decomposition of the conduction band (CB) wave functions is performed following the procedure described in Ref. [36], where the high symmetry points Γ, L and X are used as seeds for a Voronoi partition of the Brillouin zone,[37–39] having the property that each wave vector contained in that partition (Voronoi cell) is closer to the specific high-symmetry point than to any other.

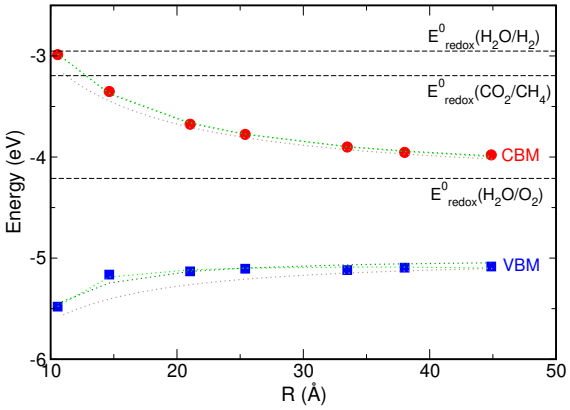

Figure 1: Valence (blue squares) and conduction (red circles) band edge energies, calculated with respect to vacuum, as a function of NC size. The dotted lines are fits to Eq. (4) (light green) and Eq. (3) (dark green). The brown dotted lines are obtained from Eq. (4) using the parameters provided by Allan et al.[40] for GaSb. The dashed lines mark the position of the redox potentials for the reduction of H_2O to H_2 (top line), the reduction of CO_2 to CH_4 (middle line), and the oxidation of H_2O to O_2 (bottom line), at pH=7. Their position relative to vacuum was obtained by shifting the values reported in Ref. [43] (Figure 2) using as a reference level our calculated position of the VBM of bulk CdSe (-5.310 eV, also confirmed experimentally[24]).

Results

Electronic structure

Although bulk GaSb emits in the infrared,[41] due to its large exciton Bohr radius NCs made of this material exhibit strong confinement even for large sizes and their photoluminescence (PL) can therefore be tuned nearly all the way up to the blue. The calculated position of the band edges (relative to vacuum) as a function of size is presented in Figure 1, showing clearly that well depths of over 1.1 eV are easily achievable in these systems. Following Williamson and Zunger[42] we fitted our data according to:

$$\begin{aligned} E_{vbm}^{dot} &= E_{vbm}^{bulk} + \frac{a}{R^{n_v}}, \\ E_{cbm}^{dot} &= E_{cbm}^{bulk} + \frac{b}{R^{n_c}} \end{aligned} \tag{3}$$

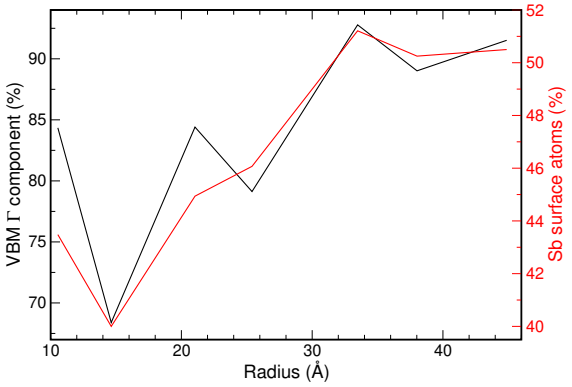

Figure 2: Γ component of the VBM (black line, left-hand y axis) and percentage of Sb surface atoms - defined as $N(Sb)_{surf}/\left[N(Sb)_{surf}+N(Ga)_{surf}\right]$ - (red line, right-hand y axis) as a function of NC size.

where $E^{dot}_{vbm/cbm}$ refer to the energy positions of the band edges in the dot, $E^{bulk}_{vbm}=-5.022$ eV, $E^{bulk}_{cbm}=-4.209$ eV, R is the NC radius, and a, b, n_v and n_c are the fitting parameters. We found $n_c=1.19$, similar to the pseudopotential value found for InAs NCs ($n_c=0.95$),[42] and $n_v=1.96$, close to the effective mass (EMA) prediction ($n_v=2$), although the fit for the size dependence of our VBM energies is not as good as that for the CBM (our fitted values for a and b are -43.21 and 20.34 respectively). Allan *et al.*[40] used a different parametrization to fit the band edges of NCs made of different III-V materials calculated with the atomistic tight-binding approach:

$$\begin{aligned} E^{dot}_{vbm} &= E^{bulk}_{vbm}-\frac{1}{a_vD^2+b_vD+c_v}, \\ E^{dot}_{cbm} &= E^{bulk}_{cbm}+\frac{1}{a_cD^2+b_cD+c_c} \end{aligned} \tag{4}$$

where $D=2R$ (in nm), and a_i, b_i and c_i ($i=v,c$) are the fitting parameters.

Our fitted cbm values ($a_c=0.02183$, $b_c=0.33855$ and $c_c=0.00604$) are close to their fitted cbm parameters ($a_c=0.02650$, $b_c=0.33745$ and $c_c=0.09540$) for the case of GaSb, whereas our vbm parameters ($a_v=-0.51288$, $b_v=7.28085$ and $c_v=-10.8934$) are very different (even in sign) from theirs ($a_v=0.08017$, $b_v=0.63268$ and $c_v=0.07146$). Unfortunately, they do not present the detailed size-dependent band edges curves for this material but only their parametrization (brown dotted lines in Figure 1). We can, therefore, only comment on the quality of agreement with the latter. As it was the case with Williamson

and Zunger's parametrization, the fit of our calculated CBM is much better than that of the VBM.

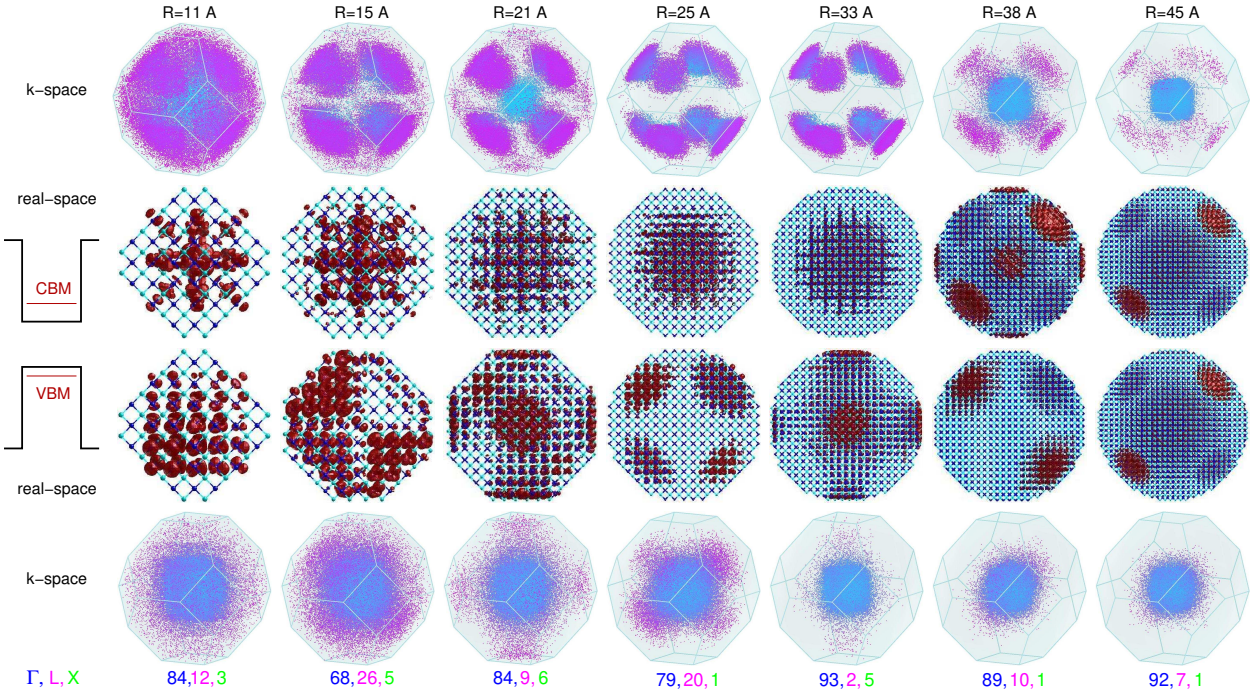

Figure 3: Calculated 3D charge densities in real space (2nd and 3rd rows) and k-space composition visualised in a 3D Brillouin zone (top and bottom rows: points close to the L points are displayed in magenta, points close to Γ are coloured in blue; the Γ, L and X components are reported below each panel) for the valence (3rd and 4th rows) and conduction (1st and 2nd rows) band edges, for all sizes considered.

Part of the reason for this poor fitting could be due to the different stoichiometry (Sb-rich both in total and also, more importantly, on the surface, as opposed to the Ga-rich composition, both in total and on the surface, which is prevalent among all other sizes) of the NCs with $R \geq 33$ Å whose VBM energies are slightly lower than expected according to Eq. (3). We find this to be a general trend in NCs, their VBM being determined by the anion: The VBM in NCs with anion-rich surfaces is always found at a lower energy than that in NCs with cation-rich surfaces. We also find (Figure 2) that a Sb-rich surface correlates with a large Γ component of the VBM and vice versa: indeed the $R = 15$ Å NC has the largest percentage of Ga surface atoms, the lowest VBM Γ component and its VBM is much higher than predicted by Eq. (3). Based on these considerations, we can speculate that the poor

agreement obtained with the curves by Allan et al.[40] (brown dotted lines in Figure 1) could originate from the fact that the structures they studied might have been cation-centered, hence exhibited Sb-rich surfaces for small sizes, leading to lower values for the VBM than our Ga-rich NCs.

It is worth mentioning that the level of accuracy required to capture such detail is not achievable with continuum methods like the popular **k·p** - which cannot distinguish between the properties of Ga-rich and Sb-rich CQDs - but is only available to atomistic methods. Most importantly, however, the **k·p** method misses the contributions from both X and L high symmetry points (at least up to the 8-band version), which, as shown in Figure 3, Figure 4, and Figure 5, are vital to understand the properties of GaSb at the nanoscale.

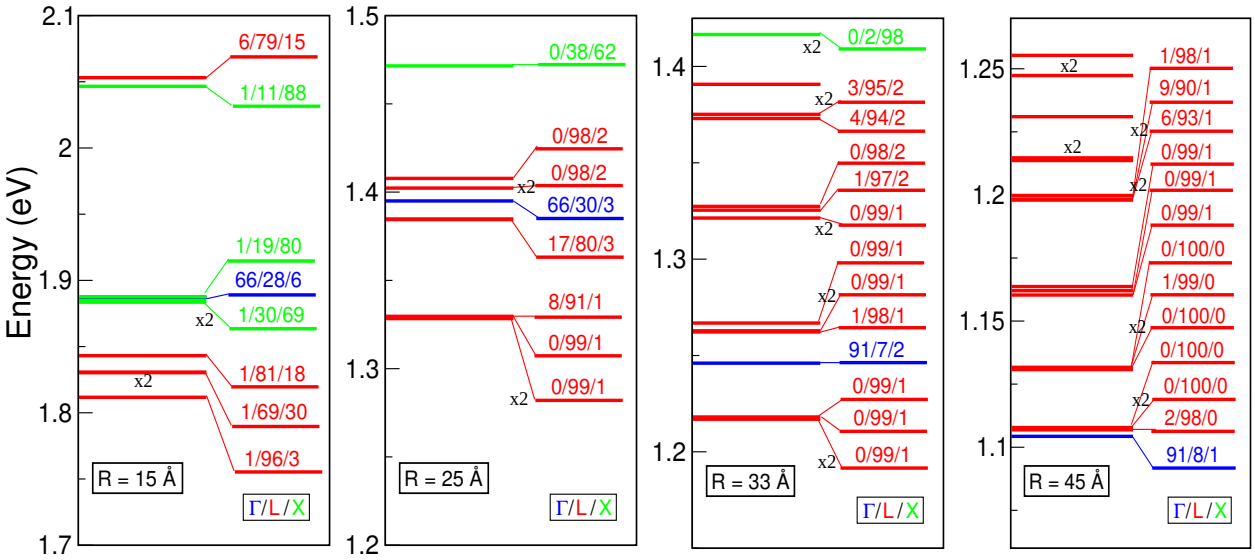

Figure 4: CB electronic structure for selected GaSb NC sizes (R = 15, 25, 33, 45 Å). Each panel displays energy levels relative to the top of the valence band (left-hand side) and k-vector decomposition (right-hand side) for a different dot size. The different states are coloured according to their main character (Γ, blue; L, red; and X, green) resulting from such a decomposition. "×N" indicates the state degeneracy.

The most interesting feature of the electronic structure of these NCs is the composition of the conduction band states (Figure 4), and more specifically of the CBM (Figure 3 and Figure 5), in terms of their k-vector components. We find that already NCs with radii as large as 36 Å experience sufficient confinement to exhibit a Γ to L transition in the CBM character,

whereas the VBM has prevalent Γ character for all sizes (Figure 3). As a consequence a direct-to-indirect band gap transition takes place at around $R = 36$ Å. We investigated the effect of 6 ligand sets with different electronegativity (see [44]) and found that such transition takes place at similar or larger sizes in all cases except for very electronegative ligands (type A in Ref. [44]), where such transition is suppressed, even for very small NCs (down to $R = 8$ Å). Figure 4 shows that with decreasing size (increasing confinement) also the X-derived states decrease in energy sufficiently to appear among the lowermost 10 conduction states, whereas, at the same time, the energy of the Γ-derived ones increases steadily.

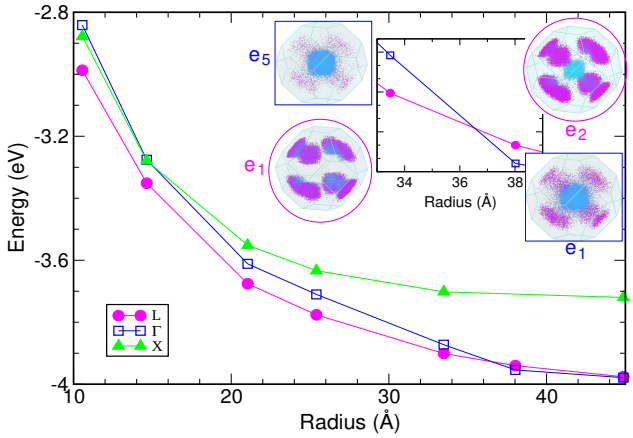

Figure 5: Lowest confined conduction band states derived from Γ (blue squares and line), L (magenta circles and line), and X (green triangles and line). The inset shows a detail of the crossing between Γ and L and the calculated k-vector decomposition of the four states represented.

Optical properties

Owing to the strong confinement experienced by these nanostructures, the emission of GaSb CQDs can be tuned from the IR, nearly all the way to the blue (for $R < 10$ Å), as can be seen from Figure 6, where we plot the calculated positions of both PL and absorption edges as a function of the nanocrystal radius. We fitted the band edge absorption according to

$$E_g^{dot} = E_g^{bulk} + \frac{A}{D^n} \tag{5}$$

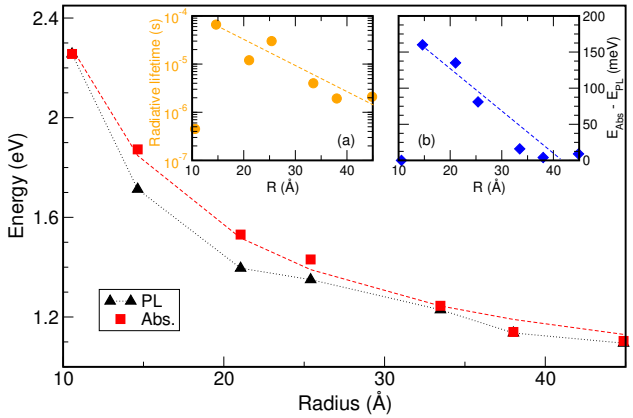

Figure 6: Optical properties as a function of size. Main panel: energy dependence on NC radius (R) of the band edge absorption (Abs., red squares - the red dashed line is a fit to the theoretical data according to Eq. (5)), and emission (PL, black triangles - the dotted line is a guide to the eye). Left inset: room temperature radiative lifetime (orange symbols) as a function of radius. Right inset: Stokes shift (energy difference between red and black symbols in the main panel) vs radius. The dashed lines are a guide to the eye.

and found $A = 38.02$ and $n = 1.07$ - red dashed line in Figure 6 - with a size dependence in stark contrast with the prediction ($n = 2$) of simple effective mass approaches,[48] but nearly identical to that found for InP ($n = 1.09$),[45,46] and similar to that found for InAs ($n = 0.9$),[42] and Si ($n = 1.18$).[47]

Large separations between emission and band edge absorption (referred to as "global Stokes shifts") suppress photoluminescence self-absorption and are therefore beneficial to all applications exploiting light emitted from the dot (LEDs, biological imaging,[49] lasers, solar energy harvesting,[50,51] etc.). Inset (b) of Figure 6 shows that the Stokes shifts achievable in these NCs range from 0 up to 160 meV, depending on the size. These shifts are also accompanied by long radiative times (inset (a) of Figure 6) on the microsecond scale (except for the smallest NC considered), due to the indirect nature of the band gap transition, discussed above.

Both radiative lifetimes and Stokes' shifts show a decreasing trend with increasing NC radius (dashed lines in insets (a) and (b) of Figure 6), except for the smallest structure considered which exhibits the fastest recombination time which is also accompanied by the smallest Stokes' shift calculated. A similar behaviour to our Stokes' shift was also found for

the dark-bright energy splitting in GaAs NCs by Luo *et al.*[52] The decrease of the radiative recombination times with increasing size is instead consistent with experiment in CdS[53] and CdSe[54,55] nanocrystals, and in contrast with the trend observed in InAs[56] and CdTe dots.[55]

In order to better understand the nature of the different transitions, we calculated the symmetry of the single-particle states involved and the resulting total symmetry of the excitons contributing to the optical transitions.[57] We find the CBM envelope function symmetry to be prevalently s-like for all sizes except for radii 25 and 33.5 Å, when it is prevalently p-like (we find that the symmetry of a state is never pure s- or pure p-like, but it always displays some degree of mixing; hence when, in what follows, we refer to l-like symmetry we always intend *prevalent* l-like symmetry), whereas the symmetry of the VBM is s-like only for the two smallest sizes ($R = 11$ and 15 Å) and p-like for all the others. As a consequence, in the smallest NC the exciton ground state is split into a lower fivefold-degenerate forbidden $\mathbb{E} + \mathbb{T}_1$ multiplet and a higher allowed threefold-degenerate $\mathbb{T}_2$, separated by only 10 meV (see Fig. S1, Supporting Information). As the width of our optical peaks is 5 times larger than this separation, the resulting Stokes shift is 0. Furthermore this size's CBM has the largest Γ component of all dots (12.4%), leading to the fastest radiative time of them all. The CBM of the 15 Å NC has nearly 0 Γ character (see Figure 4), resulting in the longest lifetime calculated here. The lifetimes then decrease with increasing size until, for $R = 38$ Å, the band edge transition becomes direct. It is therefore clear that in the case of GaSb, unlike for other III-V materials, the allowed (bright) and forbidden (dark) character of the different excitonic states (see Fig. S1, Supporting Information), hence the behaviour of their radiative lifetimes, is the result of a complex interplay between k-space composition and symmetry of the single-particle states that contribute to each exciton state.

The Stokes shifts follow the trend of the lifetimes, as a result of the progressive shift to lower energies of the fully allowed optical transitions, due to the increase in the density of single-particle states with increasing size.

The combination of visible light absorption and long recombination lifetimes ($> 0.5 \times$

10^-6 s) is ideal for many solar energy conversion applications. Here we will focus in particular on photocatalytic CO_2 reduction with water. This reaction involves three main steps: (1) photogeneration of an electron-hole pair; (2) electron and hole separation and migration to the nanocrystal surface (where a co-catalyst may be present); (3) reduction of CO_2 by the electron and oxidation of H_2O by the hole. Apart from the general improvements in efficiency due to nanostructuring (such as shortened carrier collection pathways, improved light distribution, quantum-size-confinement-induced increase in interfacial charge transfer rates, pH-tunability of interfacial charge transfer and surface-area-enhanced charge transfer),[58] the use of GaSb dots as catalyst would lead to specific major advantages in each of the above steps: (1) unlike most of the semiconductor materials used for this reaction (mainly TiO_2,[43] but also WO_3[59] and CeO_2[60]), whose bulk band gap is large (2.6-3.6 eV) the absorption of GaSb NCs can be tuned to span the whole visible spectrum, optimising light harvesting efficiency; (2) their radiative recombination lifetimes ($> 0.5 \times 10^-6$ s) are longer than (or comparable to) the typical redox reaction times ($> 10^{-8}$ s)[43] - which are usually too slow to compete with the radiative lifetimes exhibited by common semiconductor nanocrystals ($\sim 10^{-9}$ s) - hence the charge carriers in GaSb NCs would have sufficient time to reach the surface and react with CO_2 and H_2O before recombining (The efficiency of the photocatalytic reaction depends critically on the competition between these two processes, as well as on the light absorption efficiency). A recent study[44] suggests that a further over-one-order-of-magnitude increase in radiative times could be obtained by exchanging the capping group with a more electropositive ligand (throughout this work we have used passivants with intermediate electronegativity - corresponding to set D in Ref. [44]); (3) their band structure - an important aspect of the reaction is the position of the catalyst's band edges relative to the redox potential for CO_2 reduction (RP1) and H_2O oxidation to O_2 (RP2): in order for a semiconductor to be able to catalyse the reduction of CO_2 with H_2O (i) its CBM should be higher (more negative) than RP1 while (ii) the VBM should be lower (more positive) than RP2. Although all sizes considered here satisfy (ii) (see bottom dashed line in Figure 1), we

estimate that only small GaSb nanocrystals ($R \lesssim 13$ Å) would satisfy (i) in the case of the formation of CH_4 (see middle dashed line in Figure 1), which, having the least negative redox potential (-0.24 V at pH=7),[43] is the thermodynamically more favourable reduction process. In addition to these properties, the selectivity towards CO_2 reduction is a determining factor, in the presence of H_2O, as the reduction of H_2O to H_2 strongly competes with the reduction of CO_2. The former, being a two-electron reaction compared to the eight electrons needed for the formation of CH_4, is, in fact, kinetically more favourable. We find that the CBM of GaSb NCs with $R > 10$ Å, is lower than the redox potential for the reduction of H_2O to H_2 (see top dashed line in Figure 1). Water reduction is therefore expected to be suppressed in GaSb NCs simply due to their specific band structure. This represents a huge advantage compared to other semiconductor nanostructures, where some degree of surface manipulation is required to enhance the photocatalytic reduction of CO_2 in the presence of H_2O. As a consequence, unlike with TiO_2[61] or other semiconductors, in the case of GaSb the use of both solid-liquid or solid-vapour reaction modes should be possible and should yield similar rates of CH_4 formation, adding further flexibility to the design of the reactor. A further increase in the internal quantum efficiency of CO_2 reduction could be achieved with the introduction of additional smaller GaSb NCs, which would act as "sensitiser" NCs (i.e., absorb light at a slightly higher energy) and funnel the excitons, through a Förster energy transfer mechanism, to "catalyst" NCs, which, in turn, deliver the electrons to their surface for the reduction reaction. A sensitiser-to-catalyst ratio of 8:1 would provide all 8 electrons needed for the reduction of CO_2 to CH_4. A similar strategy recently led[62] to an increase of over one order of magnitude of the internal quantum efficiency of the photocatalytic reduction of H^+ to H_2 using CdSe-based NCs. The latter result proves the feasibility for our catalyst NC to accumulate multiple redox equivalents at a single catalytic site. This is made possible by the neutrality of the funnelled exciton, which can be transferred from sensitiser NC to catalyst NC without any accompanying nuclear reorganisation of either chromophores or solvent.[62] The above discussion is clearly oversimplified, as it neglects some aspects of surface modifi-

cation that may be needed to achieve efficient adsorption, activation and transformation of CO_2. Nevertheless, it provides a list of desirable properties that make GaSb NCs appealing candidates for photocatalytic applications.

Conclusions

We have presented a comprehensive theoretical characterisation of colloidal GaSb nanocrystals with radii ranging from 11 Å, to 45 Å, containing from 175 to over 13000 atoms. We have investigated the size dependence of conduction and valence band edge energies, k-space composition and symmetry of their respective wave functions, the evolution of Γ-, *L*- and *X*-derived states in the conduction band, absorption and emission spectra, radiative lifetimes and Stokes' shifts. We found GaSb nanocrystals to have a size-dependent emission tunable throughout the visible spectrum, large Stokes's shifts, and, due to a confinement-induced direct-to-indirect band gap transition occurring at very large sizes, long radiative lifetimes ($> 0.5 \times 10^{-6}$). Such properties make them promising building blocks for a wide range of applications, including solar energy conversion, memory storage and, in particular, photocatalytic CO_2 reduction, where GaSb NCs may represent a viable and more versatile alternative to the semiconductor nanostructures commonly used as catalysts. We believe that the properties highlighted in this study will stimulate renewed efforts to synthesise this new colloidal nanomaterial.

References

(1) Dutta, P. S.; Bhat, H. L.; Kumar V. The Physics and Technology of Gallium Antimonide: An Emerging Optoelectronic Material. *J. Appl. Phys.* **1997**, *81*, 5821-5870.

(2) Motosugi, G.; Kagawa, T. Temperature Dependence of the Threshold Current of AlGaAsSb/GaSb DH Lasers *Jpn. J. Appl. Phys.* **1980**, *19*, 2303.

(3) Ohmori, Y.; Tarucha, S.; Horikoshi, Y.; Okamoto, H. Room Temperature Operation of $Al_{0.17}Ga_{0.83}Sb$/GaSb Multi-Quantum Well Lasers Grown by Molecular Beam Epitaxy, *Jpn. J. Appl. Phys.* **1984**, *23*, L94-L96.

(4) Morosini, M. B. Z.; Herrera-Perez, J. L.; Loural, M. S. S.; Von Zuben, A. A. G.; da Silveira, A. C. F.; Patel, N. B. Low-Threshold GaInAsSb/GaAlAsSb Double-Heterostructure Lasers Grown by LPE *IEEE J. Quantum Electron.* **1993** *29*, 2103-2108.

(5) Hildebrand, O.; Kuebart, W.; Benz, K. W.; Pilkuhn, M. H. $Ga_{1-x}Al_xSb$ Avalanche Photodiodes: Resonant Impact Ionization with Very High Ratio of Ionization Coefficients *IEEE J. Quantum Electron.* **1981** *17*, 284-288.

(6) Hildebrand, O.; Kuebart, W.; Pilkuhn, M. H. Resonant Enhancement of Impact in $Ga_{1-x}Al_xSb$ *Appl. Phys. Lett.* **1980**, *37*, 801.

(7) Segawa, K.; Miki, H.; Otsubo, M.; Shirata, K. Coherent Gunn Oscillations in $Ga_xIn_{1-x}Sb$ *Electron. Lett.* **1976** *12*, 124-125.

(8) Hilsum, C.; Rees, H. D. Three-Level Oscillator: a New Form of Transferred-Electron Device *Electron. Lett.* **1970** *6*, 277-278.

(9) L. M. Fraas, L. M.; Girard, G. R.; Avery, J. E.; Arau, B. A.; Sundaram, V. S.; Thompson, A. G.; Gee, J. M. GaSb Booster Cells for Over 30% Efficient Solar-Cell Stacks. *J. Appl. Phys.* **1989** *66*, 3866-3870.

(10) Juang, B.-C.; Laghumavarapu, R. B.; Foggo, B. J.; Simmonds, P. J.; Lin, A.; Liang, B.; Huffaker, D. L. GaSb Thermophotovoltaic Cells Grown on GaAs by Molecular Beam Epitaxy Using Interfacial Misfit Arrays *Appl. Phys. Lett.* **2015**, *106*, 111101-1–111101-5.

(11) Kazakova, O.; Gallop, J. C.; Cox, D. C.; Brown, E.; Cuenat, A.; Suzuki, K. Opti-

mization of 2DEG InAs/GaSb Hall Sensors for Single Particle Detection. *IEEE Trans. Magn.* **2008**, *44*, 4480-4483.

(12) Ohmori, Y.; Suzuki, Y.; Okamoto, H. Room Temperature CW Operation of GaSb/AlGaSb MQW Laser Diodes Grown by MBE. *Jpn. J. Appl. Phys.*, **1985** *24*, L657-L660.

(13) Johnson, J. L.; Samoska, L. A.; Gossard, A. C.; Merz, J. L.; Jack, M. D.; Chapman, G. R.; Baumgratz, B. A.; Kosai, K.; Johnson S. M. Electrical and Optical Properties of Infrared Photodiodes Using the InAs/$Ga_{1-x}In_xSb$ Superlattice in Heterojunctions with GaSb. *J. Appl. Phys.* **1996**, *80*, 1116.

(14) M. Motyka, M.; Sek, G.; Ryczko, K.; Misiewicz, J.; Lehnhardt, T.; Höfling, S.; Forchel, A. Optical Properties of GaSb-Based Type II Quantum Wells as the Active Region of Midinfrared Interband Cascade Lasers for Gas Sensing Applications *Appl. Phys. Lett.* **2009** *94*, 251901.

(15) Babadi, A. S.; Svensson, J.; Lind, E.; Wernersson, L.-E. Impact of Doping and Diameter on the Electrical Properties of GaSb Nanowires. *Appl. Phys. Lett.* **2017** *110*, 053502.

(16) Dey, A. W.; Svensson, J.; Borg, B. M.; Ek, M.; Wernersson, L.-E. Single InAs/GaSb Nanowire Low-Power CMOS Inverter *Nano Lett.* **2012**, *12*, 5593-5597.

(17) Shterengas, L.; Belenky, G. L.; Gourevitch, A.; Donetsky, D.; Kim, J. G.; Martinelli, R. U.; Westerfeld, D. High-Power 2.3-μm GaSb-Based Linear Laser Array. *IEEE Photonics Technol. Lett.* **2004** *16*, 2218-2220.

(18) Mourad, C.; Gianardi, D.; Kaspi, R. 2 μm GaInAsSb/AlGaAsSb Midinfrared Laser Grown Digitally on GaSb by Modulated-Molecular Beam Epitaxy *J. Appl. Phys.* **2000** *88*, 5543-5546.

(19) Tomlins, P. H.; Wang, R. K. Theory, Developments and Applications of Optical Coherence Tomography. *J Phys D: Appl Phys* **2005**, *38*, 2519-2535.

(20) Marent, A.; Geller, M.; Schliwa, A.; Feise, D.; Pötschke, K.; Bimberg, D. 10^6 Years Extrapolated Hole Storage Time in GaSb/AlAs Quantum Dots *Appl. Phys. Lett.* **2007**, *91*, 242109.

(21) Geller, M.; Marent, A.; Bimberg, D. *Handbook of Nanophysics: Nanoelectronics and Nanophotonics*, K. D. Sattler (CRC Press, Boca Raton, FL.,2010), Sec.2.1.

(22) Hayne, M.; Young, R. J.; Smakman, E. P.; Nowozin, T.; Hodgson, P.; Garleff, J. K.; Rambabu, P.; Koenraad, P. M.; Marent, A.; Bonato, L.; Schliwa, A.; Bimberg, D. The Structural, Electronic and Optical Properties of GaSb/GaAs Nanostructures for Charge-Based Memory *J. Phys. D: Appl. Phys.* **2013** *46* 264001.

(23) Sala, E. M.; Stracke, G.; Selve, S.; Niermann, T.; Lehmann, M.; Schlichting, S.; Nippert, F.; Callsen, G.; Strittmatter, A.; Bimberg, D. Growth and Structure of $In_{0.5}Ga_{0.5}Sb$ Quantum Dots on GaP(001), *Appl. Phys. Lett.* **2016**, *109*, 102102.

(24) Jasieniak, J.; Califano, M.; Watkins, S. E. Size-Dependent Valence and Conduction Band-Edge Energies of Semiconductor Nanocrystals *ACS Nano* **2011**, *5*, 5888-5902.

(25) Miura, N. *Physics of Semiconductors in High Magnetic Fields* Oxford science publications, OUP Oxford, 2008, ISBN: 0198517564, 9780198517566

(26) Luo, J.-W.; Franceschetti, A.; Zunger, A. Quantum-Size-Induced Electronic Transitions in Quantum Dots: Indirect Band-Gap GaAs. *Phys. Rev. B* **2008**, *78*, 035306.

(27) Graf, P.A.; Kim, K.; Jones, W.B.; Wang, L.W. Surface Passivation Optimization Using DIRECT. *J. Comp. Phys.* **2007**, *224*, 824-835.

(28) The Pescan code and its documentation are available from http://cmsn.lbl.gov/html/Escan/DOE-nano/pescan.htm

(29) Wang, L.-W.; Zunger, A. Local-Density-Derived Semiempirical Pseudopotentials. *Phys. Rev. B* **1995**, *51*, 17 398.

(30) Magri, R.; Zunger, A. Effects of Interfacial Atomic Segregation and Intermixing on the Electronic Properties of InAs/GaSb Superlattices. *Phys. Rev. B* **2002**, *65*, 165302.

(31) Franceschetti, A.; Fu, H.; Wang, L.-W. & Zunger, A. Many-Body Pseudopotential Theory of Excitons in InP and CdSe Quantum Dots. *Phys. Rev. B* **1999**, *60*, 1819-1829.

(32) These calculations are performed using the NanoPSE suite of codes [W. B. Jones et al. *J. Phys.: Conf. Ser.* **2005**, *16*, 277-282] developed at the National Renewable Energy Lab. This computational toolset is not publicly available yet.

(33) Puangmali, T.; Califano, M.; Harrison, P. Monotonic Evolution of the Optical Properties in the Transition from Three- to Quasi-Two-Dimensional Quantum Confinement in InAs Nanorods. *J. Phys. Chem. C* **2010** *114*, 6901-6908.

(34) Califano, M.; Franceschetti, A.; Zunger, A. Temperature Dependence of Excitonic Radiative Decay in CdSe Quantum Dots: The Role of Surface Hole Traps. *Nano Lett.* **2005** *5*, 2360-2364.

(35) Dexter, D. L. *Solid State Physics*, Academic Press Inc.: New York, 1958; Vol 6, pp. 358-361.

(36) Sills, A.; Harrison, P.; Califano, M. Exciton Dynamics in InSb Colloidal Quantum Dots. *J. Phys. Chem. Lett.* **2015** *7*, 31-35

(37) Aurenhammer, F. Voronoi Diagrams - A Survey of a Fundamental Geometric Data Structure. *ACM Computing Surveys* **1991**, *23*, 345-405.

(38) Okabe, A.; Boots, B.; Sugihara, K.; Chiu, S. N. *Spatial Tessellations - Concepts and Applications of Voronoi Diagrams*. 2nd edition. John Wiley, 2000, ISBN 0-471-98635-6.

(39) Tran, Q.T.; Tainar, D.; Safar, M. *Transactions on Large-Scale Data- and Knowledge-Centered Systems*, **2009**, ISBN 9783642037214.

(40) Allan, G.; Niquet, Y. M.; Delerue, C. Quantum Confinement Energies in Zinc-Blende III-V and Group IV Semiconductors. *Appl. Phys. Lett.* **2000** *77*, 639-641.

(41) Group IV, Elements, IV-IV and III-V Compounds. Part b - Electronic, Transport, Optical and Other Properties. In *Landolt- Börnstein - Group III Condensed Matter*, Madelung, O.; Rössler, U.; Schulz, M., Eds.; Springer-Verlag: Germany, 2002; Vol. 41A1b.

(42) Williamson, A. J.; Zunger, A. Pseudopotential Study of Electron-Hole Excitations in Colloidal Free-Standing InAs Quantum Dots. *Phys. Rev. B* **1999** *61*, 1978-1991.

(43) Xie, S.; Zhang, Q.; Liu, G.; Wang, Y. Photocatalytic and Photoelectrocatalytic Reduction of CO2 Using Heterogeneous Catalysts with Controlled Nanostructures. *Chem. Commun.* **2016**, *52*, 35-59.

(44) Califano, M. Suppression of Auger Recombination in Nanocrystals via Ligand-Assisted Wave Function Engineering in Reciprocal Space *J. Phys. Chem. Lett.* **2018** *9*, 2098-2104.

(45) Fu, H.; Zunger, A. Local-Density-Derived Semiempirical Nonlocal Pseudopotentials for InP with Applications to Large Quantum Dots *Phys. Rev. B* **1997** *55*, 1642-1653.

(46) Micic, O. I.; Cheong, H. M.; Fu, H.; Zunger, A.; Sprague, J. R.; Mascarenhas, A.; Nozik, A. J. Size-Dependent Spectroscopy of InP Quantum Dots. *J. Phys. Chem. B* **1997**, *101*, 4904-4912.

(47) Reboredo, F.; Franceschetti, A.; Zunger, A. Excitonic Transitions and Exchange Splitting in Si Quantum Dots *Appl. Phys. Lett.* **1999** *75*, 2972-2974.

(48) Brus, L. E., Electron-Electron and Electron-Hole Interactions in Small Semiconductor Crystallites: The Size Dependence of the Lowest Excited Electronic State. *J. Chem. Phys.* **1984** *80*, 4403-4409.

(49) Tu, C.-C.; Awasthi, K.; Chen, K.-P.; Lin, C.-H.; Hamada, M.; Ohta, N.; Li, Y.K. Time-Gated Imaging on Live Cancer Cells Using Silicon Quantum Dot Nanoparticles with Long-Lived Fluorescence. *ACS Photonics*, **2017**, *4*, 1306-1315.

(50) Meinardi, F.; Colombo, A.; Velizhanin, K. A.; Simonutti, R.; Lorenzon, M.; Beverina, L.; Viswanatha, R.; Klimov, V. I.; Brovelli, S. Large-Area Luminescent Solar Concentrators Based on 'Stokes-Shift-Engineered' Nanocrystals in a Mass-Polymerized PMMA Matrix. *Nat. Phot.* **2014**, *8*, 392-399.

(51) Meinardi, F.; Ehrenberg, S.; Dhamo, L.; carulli, F.; Mauri, M.; Bruni, F.; Simonutti, R.; Kortshagen, U.; Brovelli, S. Highly Efficient Luminescent Solar Concentrators Based on Earth-Abundant Indirect-Bandgap Silicon Quantum Dots. *Nat. Phot.* **2017**, *11*, 177-185.

(52) Luo, J. W.; Franceschetti, A.; Zunger, A. Nonmonotonic Size Dependence of the Dark-/Bright Exciton Splitting in GaAs Nanocrystals. *Phys. Rev. B* **2009** *79*, 201301(R)

(53) Yang, B.; Schneeloch, J. E.; Pan, Z.; Furis, M.; Achermann, M. Radiative Lifetimes and Orbital Symmetry of Electronic Energy Levels of CdS Nanocrystals: Size Dependence *Phys. Rev. B* **2010** *81*, 073401.

(54) de Mello Donegá, C.; Bode, M; Meijerink, A. Size- and Temperature-Dependence of Exciton Lifetimes in CdSe Quantum Dots *Phys. Rev. B* **2006** *74*, 085320.

(55) Gong, K.; Zeng, Y.; Kelley, D. F. Extinction Coefficients, Oscillator Strengths, and Radiative Lifetimes of CdSe, CdTe, and CdTe/CdSe Nanocrystals. *J. Phys. Chem. C* **2013**, *117*, 20268-20279.

(56) Yu, P. R.; Beard, M. C.; Ellingson, R. J.; Ferrere, S.; Curtis, C.; Drexler, J.; Luiszer, F.; Nozik, A. J. Absorption Cross-Section and Related Optical Properties of Colloidal InAs Quantum Dots *J. Phys. Chem. B* **2005**, *109*, 7084-7087.

(57) Yu, P.Y.; Cardona, M. Fundamentals of Semiconductors: Physics and Materials Properties. 4th edtion. Springer Berlin Heidelberg, **2010**, ISBN 978-3-642-00709-5.

(58) Osterloh, F. E. Inorganic Nanostructures for Photoelectrochemical and Photocatalytic Water Splitting *Chem. Soc. Rev.* **2013**, *42*, 2294-2320.

(59) Chen, X.; Zhou, Y.; Liu, Q.; Li, Z.; Liu, J.; Zou, Z. Ultrathin, Single-Crystal WO_3 Nanosheets by Two-Dimensional Oriented Attachment toward Enhanced Photocatalystic Reduction of CO_2 into Hydrocarbon Fuels under Visible Light *ACS Appl. Mater. Interfaces.* **2012** *4*, 3372-3377.

(60) Li, P.; Zhou, Y.; Zhao, Z.; Xu, A.; Wang, X.; Xiao, M.; Zou, Z. Hexahedron Prism-Anchored Octahedronal CeO_2: Crystal Facet-Based Homojunction Promoting Efficient Solar Fuel Synthesis *J. Am. Chem. Soc.* **2015** *137*, 9547-9550.

(61) Xie, S.; Wang, Y.; Zhang, Q.; Deng, W.; Wang, Y. MgO- and Pt-Promoted TiO_2 as an Efficient Photocatalyst for the Preferential Reduction of Carbon Dioxide in the Presence of Water. *ACS Catal.* **2014** *4*, 3644-3653.

(62) Kodaimati, M. S.; Lian, S.; Schatz, G. C.; Weiss, E. A. Energy Transfer-Enhanced Photocatalytic Reduction of Protons within Quantum Dot Light-Harvesting-Catalyst Assemblies. *Proc. Nat. Acad. Sci.* **2018** 201805625.

Supporting Information Available

Excitonic fine structure. This material is available free of charge via the Internet at `http://pubs.acs.org`.